FEBS Letters

FEBS PRESS science publishing by scientists

Quantifying the magnitude of the oxygen artefact inherent in culturing airway cells under atmospheric oxygen versus physiological levels

Abhinav Kumar[1], Lea Ann Dailey[1], Magda Swedrowska[1], Richard Siow[2], Giovanni E. Mann[2], Gema Vizcay-Barrena[3], Matthew Arno[4], Ian S. Mudway[5,6] and Ben Forbes[1]

1 Institute of Pharmaceutical Science, King's College London, UK
2 Cardiovascular Division, British Heart Foundation Centre of Research Excellence, King's College London, UK
3 Centre for Ultrastructural Imaging, King's College London, UK
4 Genomics Centre, King's College London, UK
5 MRC-PHE Centre for Environment and Health, King's College London, UK
6 NIHR Health Protection Research Unit on Environmental Hazards at King's College London in Partnership with Public Health England, London, UK

Correspondence
I. Mudway, MRC-PHE Centre for Environment and Health, Analytical and Environmental Sciences Division, School of Biomedical Sciences, King's College London, Franklin-Wilkins Building, 150 Stamford Street, London SE1 9NH, UK
Tel: +44 0 20 7848 3895
E-mails: ian.mudway@kcl.ac.uk; ian.mudway@googlemail.com

(Received 9 October 2015, revised 23 November 2015, accepted 24 November 2015, available online 23 January 2016)

doi:10.1002/1873-3468.12026

Edited by Barry Halliwell

To date, *in vitro* studies assessing the pulmonary toxicity of inhaled particles have provided poor correlation with *in vivo* results. We explored whether this discrepancy reflected cellular adaptations in pulmonary cells cultured under atmospheric oxygen concentrations (21%) compared with *in vivo* alveolar concentrations (100 mm Hg, ~ 13%) and whether this blunted cellular responses to nanoparticle challenge. At 21% oxygen, A549 cells had augmented intracellular glutathione concentrations, with evidence of increased tolerance to CuO nanoparticles, with reduced reactive oxygen species production, blunted transcriptional responses and delayed cell death, compared to cells cultured at 13% oxygen. These data support the contention that standard cell culture conditions pre-adapt cells to oxidative insults and emphasize the necessity of ensuring normoxic conditions in model systems to improve their predictive value.

Keywords: dose; lung; nanoparticle; normoxia; oxidative stress; oxygen

The conflicting pressures of increasing demand for toxicological screening and the ethical imperative to reduce the usage of animals in safety assessment have placed an emphasis on the development of *in vitro* toxicology screens. The value of such systems is entirely dependent on their accurate prediction of *in vivo*

Abbreviations
ACTB, beta cytoskeletal actin; ANXA5, annexin A5; AP-1, activator protein 1; ATM, Ataxia Telangiectasia Mutated; CASP1, caspase 1; CAT, catalase; CHEK2, checkpoint kinase 2; CHUK, conserved helix-loop-helix ubiquitous kinase; CYP1A1, cytochrome P450, family 1, subfamily A, polypeptide 1; DHR-123, dihydrorhodamine 123; EDX-HAADF TEM, energy-dispersive X-ray spectrometry–high-angle annular dark field scanning transmission electron microscopy; GADD45B, growth arrest and DNA-damage-inducible, beta; GAPDH, glyceraldehyde-3-phosphate dehydrogenase; GCLC, glutamate-cysteine ligase catalytic subunit; GPX1, cellular glutathione peroxidase; GSH, glutathione; GSTK1, glutathione *S*-transferase kappa 1; HMOX1, Heme oxygenase 1; IL6, interleukin 6; IL8, interleukin 8; KEAP1, Kelch-like ECH-associated protein 1; LTA, lymphotoxin alpha; MDM2, mouse double minute 2, human homolog of; P53-binding protein; MIF, macrophage migration inhibitory factor; MT2A, metallothionein 2A; MTT, 3-(4,5-dimethylthiazol-2-yl)-2,5-diphenyltetrazolium bromide; NFκB, nuclear factor kappa-light-chain-enhancer of activated B cells; NOS2, inducible nitric oxide synthase; NP, nanoparticles; NQO1, NAD(P)H:quinone oxidoreductase 1; Nrf2, nuclear factor (erythroid-derived 2)-like 2 transcription factor; OPA, *O*-phthaldialdehyde; PLAA, phospholipase A2-activating protein; POLDIP3, polymerase (DNA-directed), delta interacting protein 3; ROS, reactive oxygen species; SOD1, Cu, Zn superoxide dismutase; TCA, trichloroacetic acid; TEM, transmission electron microscopy; TNF, tumour necrosis factor; XRCC1, X-ray repair cross-complementing protein 1.

responses, that is *in vitro* to *in vivo* correlation. This is exemplified in the field of nanotoxicology where the large number of nanomaterials entering the market make *in vivo* hazard and risk assessments logistically and economically impracticable, and efforts to establish best practice for *in vitro* nanotoxicology have focused on issues of nanomaterial characterization, particle dosimetry, uptake and cell model selection [1–5]. Considerable investment has also been made to develop ever more complex tissue culture systems including 2D and 3D cell cocultures to more accurately model the *in vivo* situation. Even then, applying the results from *in vitro* studies to quantitatively predict *in vivo* nanomaterial toxicity has been unsatisfactory.

In contrast, the influence of the cell culture conditions has received little attention, despite recurrent attempts in the literature to flag up significant potential artefacts inherent with standard cell culture practices [6,7]. In the respiratory tract, alveolar cells experience approximately 100 mm Hg O_2 (~ 13% O_2) [8]. Despite this, mammalian cells are typically cultured using 21% O_2, a concentration at which cell culture medium has been shown to be enriched with reactive oxygen species (ROS) [9–11]. Cultured cells that fail to adapt to this oxidative environment will not thrive, creating a selective pressure for cells with an adaptive phenotype [11–14]. Such adaption, or 'culture shock', is characterized by enhanced antioxidant defences (e.g. upregulation of superoxide dimustases, increased glutathione (GSH) synthesis), downregulation of ROS-generating enzymes (e.g. cytochrome *c* oxidase [15]) or alteration of cellular targets of oxidative damage (replacement of fumarase A and B with fumarase C in *Escherichia coli* [16] and loss of aconitase in primates [17]). We hypothesized that cells cultured under atmospheric O_2 are preconditioned to tolerate subsequent oxidative insults, such as those delivered during nanomaterial challenge and that under such conditions oxidative stress-related endpoints will be poor predictors of *in vivo* toxicity.

Previous studies examining the impact of culturing cells at varying O_2 tensions have focused on atmospheric versus tissue concentrations: 2–10% O_2 (summarized in Table S1). Overall, these studies have shown evidence of increased ROS production [18–20], altered cellular redox [21], inhibited cell growth [22], altered expression profiles [23] and increased resistance to varying cells stressors [24] in cells cultured under 21% O_2, consistent with the induction of cellular tolerance. However, the studies have tended to be limited in their scope and have focussed predominately on stem and immune cells.

We examined whether A549 cells, the most widely used airway epithelial cell model, demonstrated induction of cytoprotective antioxidant defences under standard culture conditions, and whether culture at 21% O_2 conferred protection against copper oxide nanoparticles (CuO NPs), a known inducer of cellular oxidative stress [25]. As appropriate dose setting considerations are vital to ensure the qualitative and quantitative relevance of *in vitro* or *in vivo* study results [26], we employed both realistic exposure and overload concentrations to permit comparison with the pre-existing literature. The following endpoints were examined to provide comprehensive assessment of the impact of physiological oxygen culture conditions on the toxicological responses of alveolar epithelial cells following CuO NP challenge: (A) intracellular ROS and GSH concentrations; (B) expression of genes reflecting the hierarchal cellular response to oxidative stress; encompassing (i) the induction of antioxidant/xenobiotic defences under the regulation of the nuclear factor (erythroid-derived 2)-like 2 transcription factor (Nrf2) and activator protein-1 (AP1) [27], (ii) the transition to inflammation (nuclear factor kappa-light-chain-enhancer of activated B cells, NFκB [28]) and (iii) cell arrest and apoptosis (tumour protein 53, p53 [29]) In addition, the negative regulators of each of these transcription factors were examined: Kelch-like ECH-associated protein 1 (KEAP1) for Nrf2, conserved helix-loop-helix ubiquitous kinase (CHUK) for NFκB and mouse double minute 2 homolog (MDM2) for p53, to clarify transition between these tiers of response (Fig. 1, Table S2). (C) Cell morphometry to infer between modes of cell death, particle uptake.

Materials and methods

Nanocomposite copper oxide (CuO) particles (nanocrystallite form with a diameter of 2–10 nm according to the manufacturer's data, Table S4) were from NanoScale Material Inc. (Manhattan, KS, USA). All chemicals and biological materials were purchased from Sigma-Aldrich unless stated otherwise.

Particle characterization

Nanoparticles hydrodynamic diameter and zeta potential were measured on a Malvern Nanosizer ZS. *Ex vivo* oxidative potential of CuO NP was measured by ascorbic acid depletion assay according to Kelly *et al.* [30]. The experiment was performed in triplicate and values expressed as mean ± SD $nM \cdot s^{-1}$ oxidation of ascorbic acid (Table S5).

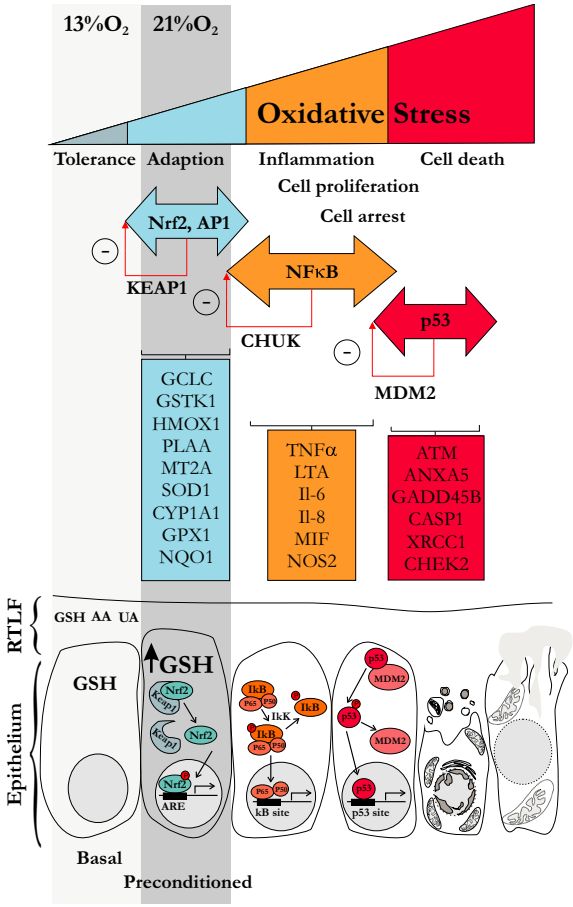

Fig. 1. Diagrammatic representation of the hierarchical response of cells to nanoparticle (NP)-induced oxidative stress at the air–lung interface, including the inherent tolerance of the airway epithelium to oxidative stress by virtue of the presence of sacrificial antioxidants (glutathione – GSH, ascorbate – AA and urate – UA) within the overlaying respiratory tract lining fluid (RTLF). When these defences are overwhelmed due to increased reactive oxygen species (ROS) production, the underlying cells initially induce adaptive strategies, illustrated by the induction of Nrf2 and AP-1, with increased intracellular GSH synthesis to mitigate against oxidative injury. The figure illustrates a number of genes known to be upregulated during this adaptive responses, as well as KEAP1, which acts as a negative regulator of Nrf2. In this study, we propose that cells cultured at 21% O_2 are effectively preconditioned against additional oxidative insults by an aberrant upregulation of cytoprotective genes relative to cells maintained under tissue relevant O_2 tensions. Under these conditions, cells are less likely to progress to more toxicologically relevant endpoints indicative of inflammation, cell arrest and apoptosis, following a NP challenge. To address this, we have examined two further panels of genes, broadly classified as being under the regulation of NFκB and p53, to reflect the transition from inflammation to cell death as the cellular oxidative burden increases. For NFκB and p53, conserved helix-loophelix ubiquitous kinase (CHUK) and MDM2 have also been studied as negative regulators of their transcriptional activity, respectively.

In vitro toxicology experiments

Human alveolar epithelial cells (A549, ATCC, USA) were cultured in an oxygen cabinet (Don Whitely Scientific Ltd, Shipley, West Yorkshire, UK) under normoxic conditions (13% O_2) and in a separate incubator under hyperoxic conditions (21% O_2). Oxygen tension in the medium prior to use was confirmed by OxyMini Oxygen Meter (WPI Inc., Hertfordshire, UK). The cells were cultured using CCMFBS10% in a humidified incubator at 37 °C and 5% CO_2. All experiments were performed on cells seeded at a density of 30 000 cells·cm^{-2} in CCMFBS2% (Fig. 2A) and NP surface area doses ranging from 0.002 to 2.0 cm^2·cm^{-2} (0.08–80 μg·mL^{-1}) were chosen based on the findings of Faux and co-workers [31] who demonstrated that 1 cm^2·cm^{-2} is a critical threshold dose at which nonspecific particle-induced inflammation occurs.

Biochemical assays

Intracellular GSH was measured by an adaptation of the original method described by Senft *et al.* [32]. ROS generation was assessed over a 4-h NP incubation period. Intracellular ROS levels were measured using dihydrorhodamine-123 in live cells using an atmosphere-controlled plate reader (BMG Labtech, Aylesbury, Bucks, UK), so as not to alter O_2 levels whist making the measurements. ROS was measured according to the methods described by Henderson *et al.* and Royall *et al.* [33,34], using dihydrorhodamine 123 at a final concentration of 20 μM (DHR-123; Sigma-Aldrich, Poole, Dorset, UK). Total protein was measured in cell lysates at the end of the experiment using the bicinchoninic acid method [35]. The effect of CuO NP on cellular metabolic activity/viability was measured by a reduction in metabolic activity and was assessed using the 3-(4,5-dimethylthiazol-2-yl)-2,5-diphenyltetrazolium bromide (MTT) assay [36].

qRT-PCR

A549 cells were seeded in six-well plate at 30 000 cells·cm^{-2}, were cultured in 13% O_2 and 21% O_2 and were treated with medium only (no NP), 8 μg·mL^{-1} and 40 μg·mL^{-1} of CuO NP. After 24 h exposure to NP, the supernatant was removed and cells were washed two times with cold (4 °C) PBS and RNA extracted using RNeasy® kits (Qiagen, Manchester, UK) following the manufacturer's instructions, and quantified with a Nanodrop® 1000 (Thermo Scientific, Hemel Hempstead, UK). qRT-PCR was carried out and data analysed using the methods described by Hofman *et al.* [37].

TEM and EDX-HAADF TEM

A549 cells were grown to confluence on 13-mm-diameter glass coverslips. For TEM, cells on coverslips were fixed,

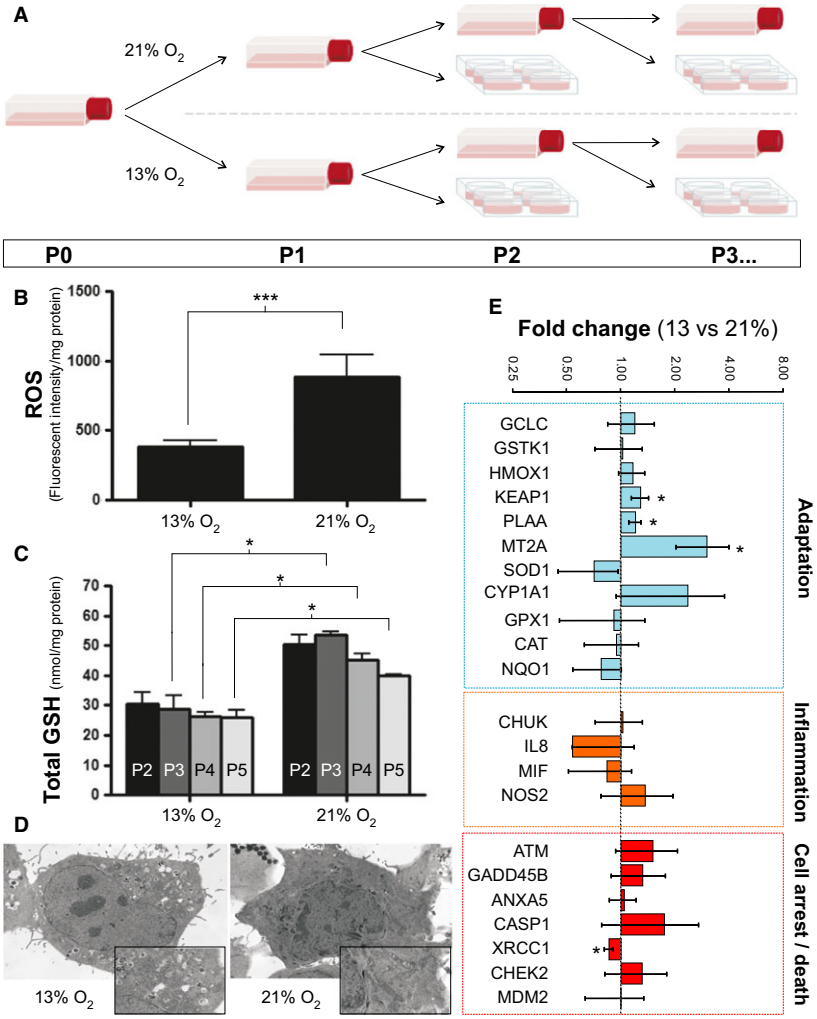

Fig. 2. Impact of oxygen tension on cellular redox and redox signalling within A549 cells. The cellular culturing scheme employed throughout this study is illustrated in panel 'A'. Initially, a single flask of A549 cells (P0) were grown to confluence at 21% O_2, prior to being divided into two equal parts for cultivation at 21% and 13% O_2, respectively (P1). All experiments in the study were subsequently performed with cells at passage numbers P2-P6 at the designated O_2 concentration. Panel 'B' illustrates the intracellular reactive oxygen species (ROS) levels (fluorescence intensity per mg protein) in A549 cells cultured under O_2 concentrations of 13% (left) and 21% (right); data represent mean ± standard deviation of duplicate experiments of $n = 3$ (***$P < 0.001$). Panel 'C' presents the intracellular glutathione (GSH) concentrations (nmol per mg protein) in A549 cells cultured under 13% (left) and 21% (right) O_2 at different passages; data represent the mean ± standard deviation of $n = 8$ experiments (*$P < 0.001$). Cellular morphologies of A549 cells cultured under the two O_2 tensions are illustrated in the representative transmission electron microscopy (TEM) images in panel 'D'. Overall morphologies at the two O_2 concentrations were equivalent, although there was evidence of increased mitochondrial length and branching in cells cultured under atmospheric O_2 (see figure inserts). The basal expression of the genes selected to illustrate the graded response of cells to oxidative stress is shown in panel 'E' (13% vs. 21% O_2). Fold change is represented as relative to the expression level in the 21% O_2 samples. The data represent $n = 3$; each performed in duplicate.

embedded in resin, sections prepared and imaged according to methods described by Hoffman *et al.* [37]. At least six images from each condition were acquired and analysed using IMAGEJ 1.47 software. Features of cellular apoptosis were assessed by visual inspection of the six representative TEM images, based on the presence of nuclear condensation (pyknosis) and fragmentation (karyorrhexis), the loss of the nucleosomes, the presence of apoptotic bodies and evidence of crescent-shaped condensed chromatin lining the nuclear membrane. Autophagic vacuoles were identified as double membranous vacuoles containing morphologically intact cytoplasmic materials [38].

Data analysis

A Student's *t*-test and one-way ANOVA were used to perform the statistical analysis. Graphical and statistical analysis was performed using GRAPHPAD PRISM version 5.00 for Windows, (GraphPad Software, San Diego, CA, USA) and IBM SPSS Statistics for Windows, Version 20.0 (IBM Corp., Armonk, NY, USA).

Results

Effect of culturing at 13 versus 21% O_2

The cell cultivation scheme to maintain cells at 21% and 13% O_2 is depicted in Fig. 2A, with experiments performed at passage numbers P2-P6. ROS generation (Fig. 2B) was assessed using the redox sensitive dye, dihydrorhodamine 123, with evidence of increased basal production at 21% O_2, consistent with previous reports [18,24]. Intracellular GSH at 21% O_2 was on average 55% higher than that observed in cells at 13% O_2 (47 ± 2 versus 26 ± 7 nmol GSH·mg protein^{-1}, respectively (Fig. 2C). Transmission electron micrographs (TEM) showed similar cell morphologies between the two culture conditions (Fig. 2D), although there was evidence of longer, extensively branched mitochondria at 21% O_2 (Fig. 2D inserts, Fig. S1), consistent with an imbalance in fission–fusion processes at 21% O_2. Increased expression of KEAP1, phospholipase A2-activating protein (PLAA) and metallothionein 2A (MT2A) was observed in cells cultured at 13% relative to 21%, whilst decreased expression (relative to 21% O_2) of X-ray repair cross-complementing protein 1 (XRCC1) was observed (Fig. 2E).

Effect of CuO NP on GSH, ROS and cell viability

To assess whether the increased GSH concentration at 21% O_2 conferred resistance to cells against oxidative stress, cells cultured at 13% and 21% O_2 were challenged with CuO NPs at increasing surface area doses (0.002–2.0 cm^2·cm^{-2}) for 6 h. Justification of the dose ranges examined is provided in the supplementary material. Under 13% O_2, a dose-dependent decrease in GSH was noted, whereas cells at 21% O_2 showed no significant reduction, except at the highest dose (2.0 cm^2·cm^{-2}) (Fig. 3A). Intracellular ROS generation over the 4-h NP incubation period in cells exposed to 0.02 cm^2·cm^{-2} CuO NP is illustrated in Fig. 3B, expressed as a % of the basal level. When the total response over time was examined, based on an analysis of the area under curve, there was a ~ 1.3-fold higher ROS production at 13% O_2 vs. 21% O_2 following the CuO NP challenge (Fig. 3B, Fig. S2). Nonparticulate challenge on ROS production using hydrogen peroxide and on GSH levels using diethyl maleate showed results consistent with our hypothesis (Fig. S3). Mitochondrial metabolic activity was also assessed using the MTT assay in cells exposed to CuO NP for 6 and 24 h (Fig. 3C). After 24 h exposure to CuO NP at 13% O_2, MTT values were 23% lower ($P = 0.06$) than the EC_{50} value observed at 21% O_2 (0.7 vs. 0.9 cm^2·cm^{-2}) at 24 h.

Effect of CuO NP on transcriptional response

Gene expression was assessed at 13% and 21% O_2 24 h after exposure to 0.2 (nonlethal approx. 8 μg·mL^{-1} ≡ 1.7 μg·cm^{-2}) and 1.0 cm^2·cm^{-2} (approx. 40 μg·mL^{-1} ~ EC_{50} ≡ 8.5 μg·cm^{-2}) doses of CuO NP. The gene expression changes associated with the dose challenges are summarized in the form of volcano plots (Fig. 3D). Of the 25 genes analysed, three (IL6, LTA and TNF) were not taken into consideration because their ΔCT value was ≥ 10. Amongst the remaining 22 transcripts analysed, 12 were statistically increased ($P < 0.05$) after CuO NPs (both doses) relative to their respective controls (Fig. 3E, Table S3).

After treatment with high dose of CuO NP (40 μg·mL^{-1}), representing an overload concentration, routinely used in numerous studies [25,39–41], a significant decrease in all the three negative regulators (KEAP-1, CHUK and MDM2) was observed (Fig. 3D) irrespective of the oxygen tension. This was consistent with activation of Nrf2, NFκB and p53, which corresponded with an increase in HMOX-1, IL8 and GADD45B expression. In contrast at the realistic exposure dose (8 μg·mL^{-1}), whilst KEAP-1 was downregulated at both 13 and 21% O_2, downregulation of CHUK and MDM2 was only apparent under normoxic conditions.

Visualization of particles and autophagic membranes within cells by TEM

Cell morphometric analysis was performed using IMAGEJ on TEM micrographs to assess a number of toxicologically relevant features, consistent with necrosis, apoptosis and autophagy: alterations in cell volume, vacuolization, changes in mitochondrial structure, nuclear condensation and the formation of autophagosomes. Examination of cell morphology by TEM 24 h after challenge with the high dose of CuO NPs demonstrated evidence of cell shrinkage and vacuolization, consistent with the induction of apoptosis at both oxygen tensions (Fig. 4A–D). Whilst both cytoplasmic (Fig. 4E) and nuclear (Fig. 4F) condensation were

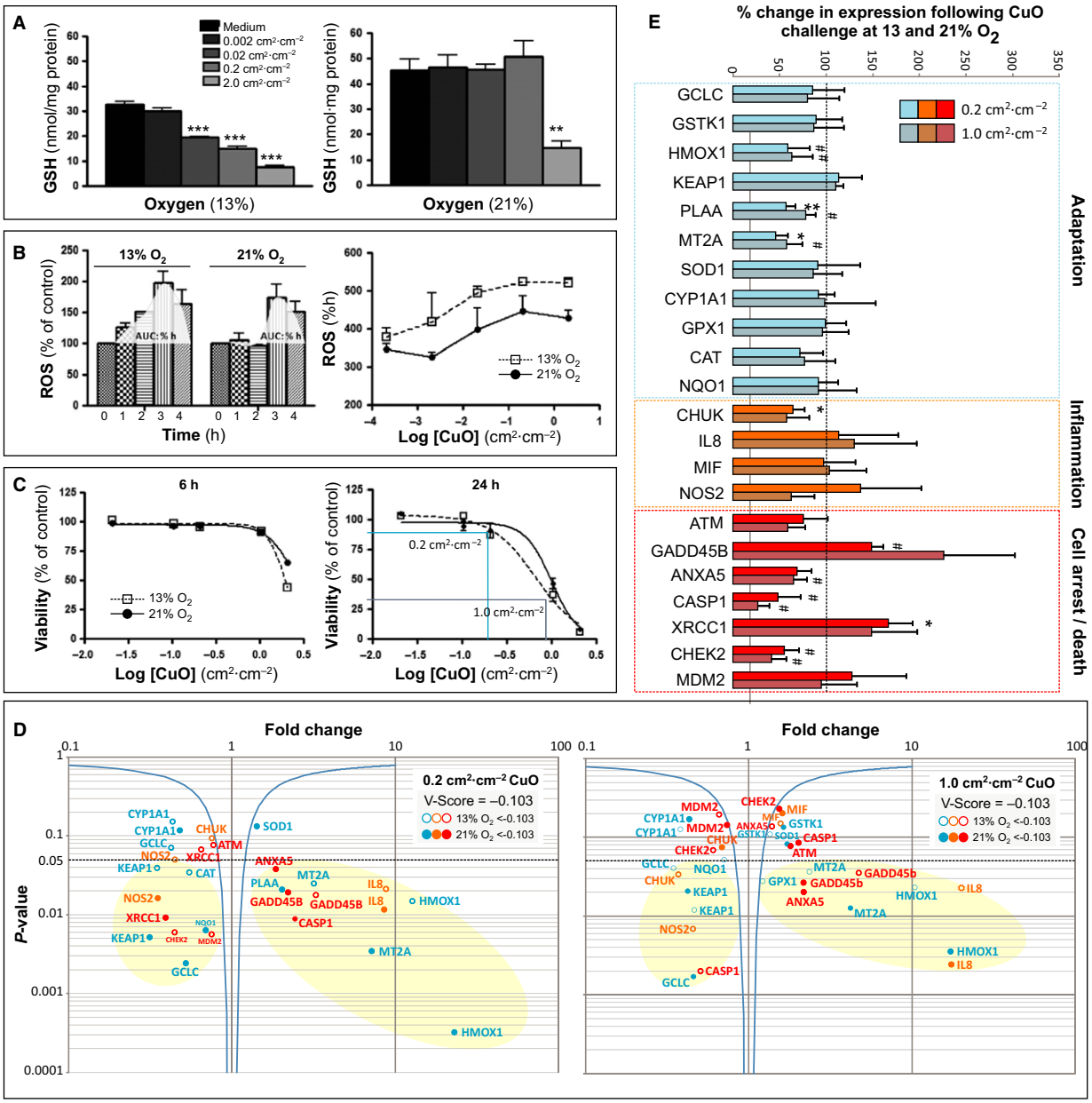

Fig. 3. Responses of A549 cells cultured under 13 or 21% O_2 to CuO nanoparticle (NP) challenge. Panel 'A' – Intracellular glutathione (GSH) (nmol per mg protein) in cells cultured under 13% (left) and 21% (right) O_2 following exposure to CuO NP at 0.002, 0.02, 0.2 and 2.0 $cm^2 \cdot cm^{-2}$ for 6 h; data represent the mean ± SD of $n = 3$ experiments (**$P < 0.01$, ***$P < 0.001$ compared to the medium control). Panel 'B' illustrates the effect of different culture conditions on reactive oxygen species (ROS) generation in A549 cells over 4 h exposure to 0.02 $cm^2 \cdot cm^{-2}$ CuO NP. The data represent duplicate experiments of $n = 3$ with the shaded areas illustrating the integrated response (AUC) over time under each challenge condition. ROS generation (% h) at each O_2 level is related to CuO NP surface area dose (0.0002–2.0 $cm^2 \cdot cm^{-2}$) in the right hand panel, providing supporting evidence ($P = 0.08$) of a blunted ROS response in cells cultured at 21% O_2. The effect of CuO NPs on the viability of A549 cells at 6 and 24 h postchallenge at 13 and 21% O_2 is illustrated in panel 'C'. Cellular metabolic activity was calculated as a percentage of the control (assay medium alone) over a surface area dose range of 0.0002–2 $cm^2 \cdot cm^{-2}$. The data represent the mean ± SD of $n = 3$; each experiment was performed in triplicate. The two selected doses taken forward for the PCR gene expression analyses are highlighted. The impact of CuO, at the low (0.2 $cm^2 \cdot cm^{-2}$ or 8 $\mu g \cdot mL^{-1}$) and high dose (1 $cm^2 \cdot cm^{-2}$ or 40 $\mu g \cdot mL^{-1}$) on gene expression 24 h postchallenge, is illustrated in the volcano plots in panel 'D'. The threshold of the volcano score using the fold change and *P*-value is illustrated by solid blue line. The observed fold change in NP-treated cells relative to their non-NP-treated controls (logarithmic scale) at 13% (open circles) and 21% O_2 (filled circles) is represented on *x*-axis and statistical significance is represented on *y*-axis. Statistical analysis was carried out using Student's *t*-test (paired, two tailed): #$P < 0.10$, *$P < 0.05$ and **$P < 0.01$.

apparent, this did not differ significantly when examined morphometrically between the two O_2 concentrations. Evidence was also obtained demonstrating more advanced apoptosis at 13% vs. 21% O_2, with increased karyorrhexis, formation of apoptotic bodies and nucleosomal loss (Fig. 4G). There were also significantly more vacuoles at 13% compared to 21% O_2, both by number and volume (Fig. 4H,I), with clear evidence of CuO NP inclusions in the vacuoles concluded from energy-dispersive X-ray spectroscopy–high-angle annular dark field (EDX-HAADF) TEM (Fig. 4J), and a greater proportion of early and late autophagosomes observed at 13% O_2 (Fig. 4K).

Discussion

This 'point of principle' work focused on the commonly employed A549 cell line providing evidence of antioxidant adaptations in cells cultured under 13% and 21% O_2. Cells cultured at 13% O_2 demonstrated a significant decrease in intracellular GSH as compared to cells cultured at 21% O_2. However, GSH data in tissue biopsies from healthy volunteers have demonstrated five times lower intracellular GSH concentration of 11.2 ± 0.6 nmol GSH·mg protein^{-1} [42]. Culturing A549 cells at 21% O_2 was not associated with an increased expression of the glutamate-cysteine ligase catalytic subunit (GCLC), suggesting other mechanisms were accounting for the elevated GSH concentration. The absence of increased transcription of GCLC, GPX1 or CAT is consistent with the findings of Yan *et al.* [43] who did not notice a change in basal mitochondrial ROS in primary hepatocytes cultured at 10% and 21% oxygen. A hypothesis to explain the elevated GSH in cells cultured at 21% O_2 may be the increased induction of cystine transport activity as demonstrated by Bannai *et al.* [44] in human fibroblasts cultured at 3% O_2 and 40% O_2 leading to a 50% increase in cystine transport activity. Cystine is rapidly reduced to cysteine which is mainly incorporated into GSH; thus, the increased transport of cystine provides may explain the elevated intracellular GSH levels observed in cells cultured at 21% O_2.

To further augment our hypothesis of antioxidant adaptation, we examined the impact of nonparticulate oxidative stress inducer hydrogen peroxide (2.5 μM; Fig. S3) on the cells. At the examined concentrations, we found that hydrogen peroxide generated increased oxidative stress (~ 166 ± 14% of medium control) in the A549 cells cultured at 13% O_2 as compared to minimal oxidative stress (~ 129 ± 8% of medium control) at 21% O_2. After extensive literature search, the authors have failed to find a reference where induction of ROS generation has been demonstrated in A549 cells using hydrogen peroxide at concentrations below 100 μM [45,46] (a 40-fold higher concentration than used by the authors). We also examined the capacity of the thiol-reactive electrophile diethyl maleate (100 μM) to deplete intracellular GSH levels (Fig. S3). After a 2-h treatment of A549 cells at 13% O_2 with diethyl maleate, we found a 25% reduction GSH as compared to negligible change in GSH in A549 cells treated at 21% O_2. Comparing our results to those reported in the literature shows that most of the studies have observed depletion of GSH in A549 cells after treatment with 1 mM diethyl maleate [47,48] and showed no effect on GSH at 125 μM.

The impact of this augmented antioxidant defence of cells on NP toxicity was examined further because induction of oxidative stress and subsequent inflammation present the best paradigm for particle toxicity [49]. Additionally, nanotoxicology is becoming increasingly important as more and more nanotechnological products enter the market. Thus, cells cultured under at 13% O_2 and 21% O_2 were challenged with increasing concentrations of CuO NP. The results demonstrated a concentration-dependent decrease in GSH, elevated ROS and decreased cell viability compared to cells cultured at 21% O_2 and challenged with CuO NP. ROS was measured using DHR-123 which has been demonstrated to react with superoxide, hydrogen peroxide, singlet oxygen and peroxynitrite per manufacturer's data. This was consistent with previous observations in antigen-challenged human T cells cultured at 5 and 20% O_2 [21]. The authors cultured T cells in freshly isolated human peripheral blood mononuclear cells and determined the GSH/GSSG ratio after 3 days in culture. They found a significantly higher ratio at physiological O_2 (5%) than at atmospheric O_2 (21%) ($P = 0.003$), which suggested that the redox status of cells cultured at physiological O_2 is more like that expected for healthy T cells *in vivo*. Measurement of ROS (ROS) and nitric oxide (NO) after antigenic stimulation by CD3/CD28 showed that T cells cultured under physiological oxygen demonstrated significantly higher (1.5- to twofold $P < 0.001$) ROS and NO production as compared to cells cultured under atmospheric oxygen.

The increased sensitivity of A549 cells cultured at 13% O_2 to CuO NP challenge can be explained by the decreased intracellular GSH level. This hypothesis would be consistent with the results obtained by Zhao *et al.* [50]. and Liu *et al.* [51]. who showed that gold NPs caused significantly more cytotoxicity on A549 cells pretreated with L-buthionine sulfoximine to decrease the expression of GSH. Recently, Liu *et al.*

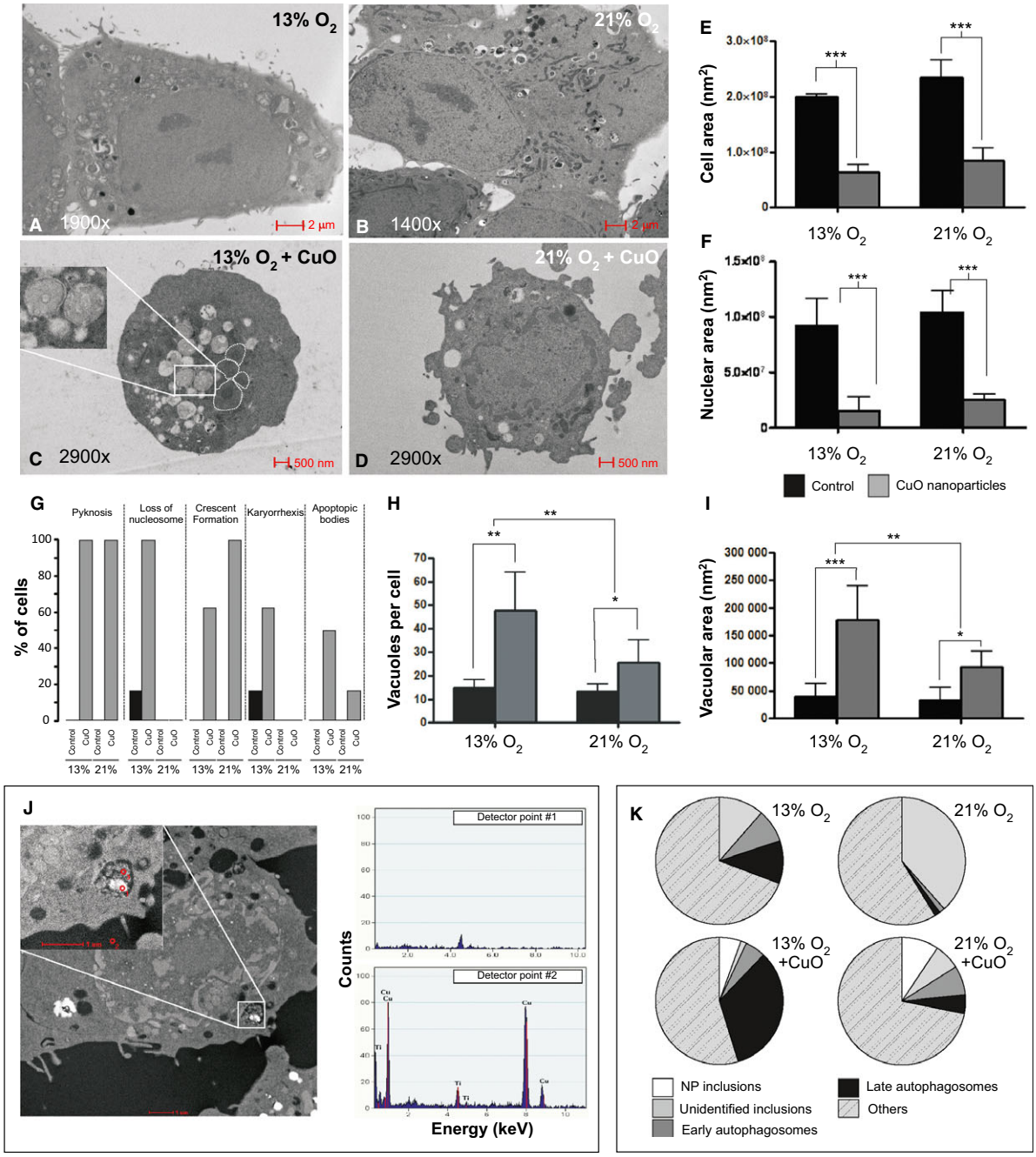

Fig. 4. Morphological analysis of CuO nanoparticle (NP)-challenged cells cultured under 13 and 21% O_2. Panels A–D present representative transmission electron microscopy (TEM) images of A549 cells cultured at 13 and 21% O_2, with (C, D) and without (A, B) co-incubation with CuO NPs (1 $cm^2 \cdot cm^{-2}$) for 24 h. The inset in panel 'C' highlights evidence of autophagosomes with double membranes and cytoplasmic inclusions. The average cellular and nuclear areas (nm^2) of A549 cells cultured under each exposure condition are illustrated in panels 'E' and 'F', respectively. Data represent the mean ± SD of six cells (***$P < 0.001$). Evidence of apoptosis through examination of nuclear morphology is presented in panel 'G' based on analyses of six representative TEM images. Panel 'H' presents the average number of vacuoles per cell (left), with panel 'I' illustrating the average vacuolar area (nm^2). Vacuoles were defined as being membrane bound, with an area above 0.01% of the total cell area and circularity between 0.09 and 1.00. Data represent the mean ± SD of $n = 6$ images (*$P < 0.05$, **$P < 0.01$, ***$P < 0.001$). Panel 'J' is a HAADF image of A549 cells and the Cu inclusion in a vacuole shows up bright. A higher magnification image of the vacuole is shown in the inset. Analysis of the particle by EDS confirmed the particle contained Cu (lower spectrum). Cu was absent from an adjacent area of analysis (upper spectrum). Panel 'K' quantifies the type of vacuoles identified under each of the exposure conditions, highlighting the increased number of early and late autophagosomes observed following CuO NP challenge in cells maintained in 13% O_2.

[52]. also demonstrated that knock-down of GCLC by siRNA in A549 cells caused a significant decrease in GSH concentrations and the treatment of GCLC siRNA-transfected cells with gold NPs caused increased ROS production, mitochondrial depolarization and activation of caspase-3. Further, it has been demonstrated that an aggressive tumour can be sensitive to drugs using a therapy based on the modulation of GSH levels in cancer cells [53]. Thus, both the non-particulate challenges further support our stated hypothesis that cells cultured under atmospheric oxygen demonstrate blunted response to oxidative stress inducing challenges perhaps due to increased intracellular GSH levels.

qRT-PCR was used to examine the oxidative stress paradigm of NP toxicity. Consistent with the downregulation of KEAP-1 under both oxygen concentrations, HMOX-1 was significantly increased at this low dose (8 $\mu g \cdot mL^{-1}$). Decreased expression of GCLC, NOS2 and CYP1A1 was also seen at this dose under both oxygen condition, in agreement with the results obtained by other authors after oxidative stress challenge [54–56], with increased IL-8 and GADD45B also apparent at 13 and 21% O_2. We would like to highlight that the similarity in transcriptional response observed is the case only at a high dose of 40 $\mu g \cdot mL^{-1}$ of copper oxide NP treatment (Fig. 3D,E). However, at a realistic exposure dose of 8 $\mu g \cdot mL^{-1}$, we observed significant downregulation of all the three negative regulators (KEAP-1, CHUK and MDM2) which would imply activation of Nrf2, NFκB and p53 in cells cultured and exposed at 13% O_2. In contrast, cells cultured at 21% O_2 demonstrate the significant decrease in KEAP-1 only thus supporting our hypothesis that atmospheric oxygen culture condition produces blunted toxicological responses to nanoparticulate challenge. An important caveat in interpreting these results is that a proportion of the observed response may be attributable to the dissolution of Cu ions from the CuO NP. However, previous studies using whole human genome array have demonstrated that the Cu ions derived from CuO NPs contribute minimally to the observed transcriptional response at doses threefold greater than our lowest employed NP concentration [57].

Transmission electron microscopy (TEM) was used to assess the morphological changes and autophagy in cells treated with CuO NP. Currently, assessment of autophagy through the identification of double membrane autophagosomes by TEM is regarded as the gold standard in mammalian cells [38]. We have therefore not examined additional confirmatory markers of autophagy such as microtubule-associated protein 1A/1B-light chain 3 (LC3)-phosphatidylethanolamine conjugate (LC3-II). Results obtained from TEM analysis showed increased cellular vacuolization, nuclear shrinkage and NP inclusion in the cells. The cells cultured at 13% oxygen further showed the presence of various autophagic structures. These results are consistent with the review by Stern *et al.* [58]. who have argued that autophagy and lysosomal dysfunction are possible mechanisms of nanomaterial-induced toxicity. Collectively, the morphological and transcriptomic data suggest that the cells at 13% O_2 were further progressed along the apoptotic pathway, with some evidence of autophagy induction.

The results obtained with NPs in this proof of concept study have more general implications as oxygen plays a fundamental role in cell metabolism and functioning. The importance of the cell microenvironment makes it vitally important that there should be a tight control of *in vitro* experimental conditions. Carreau *et al.* [59]. recently reviewed the influence of oxygen tension on molecular function and subsequent cellular behaviour and reported that cell activity is modulated by oxygen from the gene level to the proteome expression with a fine regulation. Additionally, Grodzki *et al.* [60]. demonstrated that THP-1 macrophages cultured at physiological oxygen tension (5% O_2) showed significant decrease in phagocytosis of *E. coli* particles compared to cells cultured at atmospheric oxygen. Further, Tiede *et al.* [24]. demonstrated that primary neurons cultured at physiological oxygen showed higher mitochondrial polarization, lower rates of ROS production, larger mitochondrial networks, greater cytoplasmic fractions of mitochondria and larger mitochondrial perimeters than those cultured at higher oxygen levels. Additionally, the authors also showed that cells cultured at physiological oxygen were more susceptible to HIV virotoxin challenge compared to cells cultured at atmospheric oxygen. Our data along with these observations imply that there is a general potential for cells cultured under hyperoxia to display aberrant responses in toxicity screening, impairing their *in vitro* to *in vivo* relevance.

Conclusions

We have demonstrated that cells cultured at 13% O_2 had lower intracellular GSH levels and were more sensitive to NP challenge, demonstrating perturbation in antioxidant defences to concentrations as low as 0.8 $\mu g \cdot mL^{-1}$ (~ 0.17 $\mu g \cdot cm^{-2}$), where as cells cultured at 21% O_2 only responded at overload concentrations, that is conditions which would be an unrealistic for *in vivo* exposure. These data support the contention that culturing alveolar epithelial cells under atmo-

spheric O_2 induces protective antioxidant adaptations that modify their subsequent response to NP challenge, with evidence of delayed cell death and altered gene expression related to DNA repair, cell arrest and apoptosis. We speculate that this effect is likely to be even more pronounced in primary cells, which have differentiated and reside at 13% O_2 *in vivo*. In support of this suggestion, A549 cell GSH concentrations at 13% O_2, although trending towards concentrations measured *in vivo*, were still double those observed in freshly obtained human bronchial biopsies. Whilst the data only examine discrete windows of challenge and response we feel, they highlight the fact that the artefact of culturing cells *in vitro* at an unrealistic oxygen condition renders them insensitive to subtle changes induced by realistic exposure dose of nanomaterials.

Clearly there are numerous other issues that impact on the *in vivo* relevance of *in vitro* models, including appropriateness of cell lines, submerged versus air–liquid interface exposures, monoculture versus coculture. However, oxygen tension has received minimal attention generally, and surprisingly none in the respiratory field where induction of oxidative stress pathways has been invoked as central to inhaled NP toxicity. Our data present a warning flag and emphasize the need to further characterize and understand the implications of the artefact inherent in studying cell response pathways under inappropriate oxygen tensions.

Acknowledgements

AK is funded by the EPSRC-Unilever through a Dorothy Hodgkin Postgraduate CASE Award. We thank Don Whitley Scientific Ltd for enabling this study to be conducted in their oxygen-regulated workstation. We are also grateful to Dr Alice Warley and Dr Gema Vizcay-Barrena at the Centre for Ultrastructural Imaging for their assistance with the TEM imaging.

Author contributions

AK performed cell culture and NP challenge experiments, experimental design, redox chemistry, transcriptomics, data analysis, manuscript preparation, statistical analysis and morphometry analysis. LAD performed experimental design, data analysis and manuscript preparation. MS performed cell culture and data analysis. RS and GEM performed manuscript preparation and experimental design. GVB performed the electron microscopy. MA performed manuscript preparation and transcriptomics. ISM performed experimental design, redox chemistry, transcriptomics, data analysis, manuscript preparation, statistical analysis and morphometry analysis. BF performed experimental design, data analysis and manuscript preparation.

References

1 Tantra R and Shard A (2013) We need answers. *Nat Nanotechnol* **8**, 71.
2 Fadeel B and Savolainen K (2013) Broaden the discussion. *Nat Nanotechnol* **8**, 71.
3 Lison D and Huaux F (2011) In vitro studies: ups and downs of cellular uptake. *Nat Nanotechnol* **6**, 332–333.
4 Clift MJD, Gehr P and Rothen-Rutishauser B (2011) Nanotoxicology: a perspective and discussion of whether or not in vitro testing is a valid alternative. *Arch Toxicol* **85**, 723–731.
5 Nature Nanotechnology Editorial (2012) Join the dialogue. *Nat Nanotechnol* **7**, 545.
6 Halliwell B (2003) Oxidative stress in cell culture: an under-appreciated problem? *FEBS Lett* **540**, 3–6.
7 Halliwell B (2014) Cell culture, oxidative stress, and antioxidants: avoiding pitfalls. *Biomed J* **37**, 99–105.
8 Ward JPT (2008) Oxygen sensors in context. *Biochim Biophys Acta* **1777**, 1–14.
9 de Groot H and Littauer A (1989) Hypoxia, reactive oxygen, and cell injury. *Free Radic Biol Med* **6**, 541–551.
10 Grzelak A, Rychlik B and Bartosz G (2001) Light-dependent generation of reactive oxygen species in cell culture media. *Free Radic Biol Med* **30**, 1418–1425.
11 Halliwell B and Gutteridge J (2007) Free Radicals in Biology and Medicine, 4th edn. Oxford University Press, Oxford, UK.
12 Aerts C, Wallaert B and Voisin C (1992) In vitro effects of hyperoxia on alveolar Type II pneumocytes: inhibition of glutathione synthesis increases hyperoxic cell injury. *Exp Lung Res* **18**, 845–861.
13 Halliwell B (1996) Free radicals, proteins and DNA: oxidative damage versus redox regulation. *Biochem Soc Trans* **24**, 1023–1027.
14 Halliwell B (2000) The antioxidant paradox. *Lancet* **355**, 1179–1180.
15 Campian JL, Qian M, Gao X and Eaton JW (2004) Oxygen tolerance and coupling of mitochondrial electron transport. *J Biol Chem* **279**, 46580–46587.
16 Liochev SI and Fridovich I (1993) Modulation of the fumarases *of Escherichia coli* in response to oxidative stress. *Arch Biochem Biophys* **301**, 379–384.
17 Morton RL, Iklé D and White CW (1998) Loss of lung mitochondrial aconitase activity due to hyperoxia in bronchopulmonary dysplasia in primates. *Am J Physiol* **274**, L127–L133.
18 Boregowda SV, Krishnappa V, Chambers JW, Lograsso PV, Lai W-T, Ortiz LA and Phinney DG (2012) Atmospheric oxygen inhibits growth and

differentiation of marrow-derived mouse mesenchymal stem cells via a p53-dependent mechanism: implications for long-term culture expansion. *Stem Cells* **30**, 975–987.
19 Nasto LA, Robinson AR, Ngo K, Clauson CL, Dong Q, St Croix C, Sowa G, Pola E, Robbins PD, Kang J *et al.* (2013) Mitochondrial-derived reactive oxygen species (ROS) play a causal role in aging-related intervertebral disc degeneration. *J Orthop Res* **31**, 1150–1157.
20 Villeneuve L, Tiede LM, Morsey B and Fox HS (2013) Quantitative proteomics reveals oxygen-dependent changes in neuronal mitochondria affecting function and sensitivity to rotenone. *J Proteome Res* **12**, 4599–4606.
21 Atkuri KR, Herzenberg LA, Niemi A-K, Cowan T and Herzenberg LA (2007) Importance of culturing primary lymphocytes at physiological oxygen levels. *Proc Natl Acad Sci USA* **104**, 4547–4552.
22 Forristal CE, Wright KL, Hanley NA, Oreffo ROC and Houghton FD (2010) Hypoxia inducible factors regulate pluripotency and proliferation in human embryonic stem cells cultured at reduced oxygen tensions. *Reproduction* **139**, 85–97.
23 Rinaudo PF, Giritharan G, Talbi S, Dobson AT and Schultz RM (2006) Effects of oxygen tension on gene expression in preimplantation mouse embryos. *Fertil Steril* **86**, 1252–1265, 1265.e1–e36.
24 Tiede LM, Cook EA, Morsey B and Fox HS (2011) Oxygen matters: tissue culture oxygen levels affect mitochondrial function and structure as well as responses to HIV viroproteins. *Cell Death Dis* **2**, e246.
25 Karlsson HL, Cronholm P, Gustafsson J and Möller L (2008) Copper oxide nanoparticles are highly toxic: a comparison between metal oxide nanoparticles and carbon nanotubes. *Chem Res Toxicol* **21**, 1726–1732.
26 Oberdörster G (2010) Safety assessment for nanotechnology and nanomedicine: concepts of nanotoxicology. *J Intern Med* **267**, 89–105.
27 Cho H-Y and Kleeberger SR (2010) Nrf2 protects against airway disorders. *Toxicol Appl Pharmacol* **244**, 43–56.
28 Karin M, Cao Y, Greten FR and Li Z-W (2002) NF-kappaB in cancer: from innocent bystander to major culprit. *Nat Rev Cancer* **2**, 301–310.
29 Bullock AN and Fersht AR (2001) Rescuing the function of mutant p53. *Nat Rev Cancer* **1**, 68–76.
30 Kelly F, Anderson HR, Armstrong B, Atkinson R, Barratt B, Beevers S, Derwent D, Green D, Mudway I and Wilkinson P (2011) The impact of the congestion charging scheme on air quality in London. Part 2. Analysis of the oxidative potential of particulate matter. *Res Rep Health Eff Inst* **155**, 73–144.
31 Faux SP, Tran C-L, Miller BG, Jones AD, Monteiller C, and Donaldson K (2003) In vitro determinants of particulate toxicity: The dose-metric for poorly soluble dusts. *Health and Safety Research Report* 154.
32 Senft AP, Dalton TP and Shertzer HG (2000) Determining glutathione and glutathione disulfide using the fluorescence probe *O*-phthalaldehyde. *Anal Biochem* **280**, 80–86.
33 Royall JA and Ischiropoulos H (1993) Evaluation of 2′,7′-dichlorofluorescin and dihydrorhodamine 123 as fluorescent probes for intracellular H2O2 in cultured endothelial cells. *Arch Biochem Biophys* **302**, 348–355.
34 Henderson LM and Chappell JB (1993) Dihydrorhodamine 123: a fluorescent probe for superoxide generation? *Eur J Biochem* **217**, 973–980.
35 Smith PK, Krohn RI, Hermanson GT, Mallia AK, Gartner FH, Provenzano MD, Fujimoto EK, Goeke NM, Olson BJ and Klenk DC (1985) Measurement of protein using bicinchoninic acid. *Anal Biochem* **150**, 76–85.
36 Mosmann T (1983) Rapid colorimetric assay for cellular growth and survival: application to proliferation and cytotoxicity assays. *J Immunol Methods* **65**, 55–63.
37 Hoffman E, Kumar A, Kanabar V, Arno M, Preux L, Millar V, Page C, Collins H, Mudway I, Dailey LA *et al.* (2015) Differentiating macrophage responses to inhaled medicines using a hierarchical in vitro screening strategy. *Mol Pharm* **12**, 2675–2687.
38 Eskelinen E-L (2008) To be or not to be? Examples of incorrect identification of autophagic compartments in conventional transmission electron microscopy of mammalian cells. *Autophagy* **4**, 257–260.
39 Moschini E, Gualtieri M, Colombo M, Fascio U, Camatini M and Mantecca P (2013) The modality of cell-particle interactions drives the toxicity of nanosized CuO and TiO_2 in human alveolar epithelial cells. *Toxicol Lett* **222**, 102–116.
40 Semisch A, Ohle J, Witt B and Hartwig A (2014) Cytotoxicity and genotoxicity of nano – and microparticulate copper oxide: role of solubility and intracellular bioavailability. *Part Fibre Toxicol* **11**, 10.
41 Ahamed M, Siddiqui MA, Akhtar MJ, Ahmad I, Pant AB and Alhadlaq HA (2010) Genotoxic potential of copper oxide nanoparticles in human lung epithelial cells. *Biochem Biophys Res Commun* **396**, 578–583.
42 Cook JA, Pass HI, Iype SN, Friedman N, DeGraff W, Russo A and Mitchell JB (1991) Cellular glutathione and thiol measurements from surgically resected human lung tumor and normal lung tissue. *Cancer Res* **51**, 4287–4294.
43 Yan H-M, Ramachandran A, Bajt ML, Lemasters JJ and Jaeschke H (2010) The oxygen tension modulates acetaminophen-induced mitochondrial oxidant stress and cell injury in cultured hepatocytes. *Toxicol Sci* **117**, 515–523.

44 Bannai S, Sato H, Ishii T and Sugita Y (1989) Induction of cystine transport activity in human fibroblasts by oxygen. *J Biol Chem* **264**, 18480–18484.
45 Rahman I, Gilmour PS, Jimenez LA and MacNee W (2002) Oxidative stress and TNF-alpha induce histone acetylation and NF-kappaB/AP-1 activation in alveolar epithelial cells: potential mechanism in gene transcription in lung inflammation. *Mol Cell Biochem* **234–235**, 239–248.
46 Ferlazzo N, Visalli G, Smeriglio A, Cirmi S, Lombardo GE, Campiglia P, Di Pietro A and Navarra M (2015) Flavonoid fraction of orange and bergamot juices protect human lung epithelial cells from hydrogen peroxide-induced oxidative stress. *Evid Based Complement Alternat Med* **2015**, 957031.
47 Horton ND, Biswal SS, Corrigan LL, Bratta J and Kehrer JP (1999) Acrolein causes inhibitor kappab-independent decreases in nuclear factor kappaB activation in human lung adenocarcinoma (A549) cells. *J Biol Chem* **274**, 9200–9206.
48 Yang X, Wu X, Choi YE, Kern JC and Kehrer JP (2004) Effect of acrolein and glutathione depleting agents on thioredoxin. *Toxicology* **204**, 209–218.
49 Nel A, Xia T, Mädler L and Li N (2006) Toxic potential of materials at the nanolevel. *Science* **311**, 622–627.
50 Zhao Y, Gu X, Ma H, He X, Liu M and Ding Y (2011) Association of glutathione level and cytotoxicity of gold nanoparticles in lung cancer cells. *J Phys Chem C* **115**, 12797–12802.
51 Liu M, Gu X, Zhang K, Ding Y, Wei X, Zhang X and Zhao Y (2013) Gold nanoparticles trigger apoptosis and necrosis in lung cancer cells with low intracellular glutathione. *J Nanopart Res* **15**, 1745.
52 Liu M, Zhao Y and Zhang X (2015) Knockdown of glutamate cysteine ligase catalytic subunit by siRNA causes the gold nanoparticles-induced cytotoxicity in lung cancer cells. *PLoS One* **10**, e0118870.
53 Diehn M, Cho RW, Lobo NA, Kalisky T, Dorie MJ, Kulp AN, Qian D, Lam JS, Ailles LE, Wong M *et al.* (2009) Association of reactive oxygen species levels and radioresistance in cancer stem cells. *Nature* **458**, 780–783.
54 Mani M and Khaghani S, Gol Mohammadi T, Zamani Z, Azadmanesh K, Meshkani R, Pasalar P, Mostafavi E (2013) Activation of Nrf2-antioxidant response element mediated glutamate cysteine ligase expression in hepatoma cell line by homocysteine. *Hepat Mon* **13**, e8394.
55 Dijkstra G, Blokzijl H, Bok L, Homan M, van Goor H, Faber KN, Jansen PLM and Moshage H (2004) Opposite effect of oxidative stress on inducible nitric oxide synthase and haem oxygenase-1 expression in intestinal inflammation: anti-inflammatory effect of carbon monoxide. *J Pathol* **204**, 296–303.
56 Morel Y and Barouki R (1998) Down-regulation of cytochrome P450 1A1 gene promoter by oxidative stress. Critical contribution of nuclear factor 1. *J Biol Chem* **273**, 26969–26976.
57 Hanagata N, Zhuang F, Connolly S, Li J, Ogawa N and Xu M (2011) Molecular responses of human lung epithelial cells to the toxicity of copper oxide nanoparticles inferred from whole genome expression analysis. *ACS Nano* **5**, 9326–9338.
58 Stern ST, Adiseshaiah PP and Crist RM (2012) Autophagy and lysosomal dysfunction as emerging mechanisms of nanomaterial toxicity. *Part Fibre Toxicol* **9**, 20.
59 Carreau A, El Hafny-Rahbi B, Matejuk A, Grillon C and Kieda C (2011) Why is the partial oxygen pressure of human tissues a crucial parameter? Small molecules and hypoxia. *J Cell Mol Med* **15**, 1239–1253.
60 Grodzki ACG, Giulivi C and Lein PJ (2013) Oxygen tension modulates differentiation and primary macrophage functions in the human monocytic THP-1 cell line. *PLoS One* **8**, e54926.

Supporting information

Additional supporting information may be found in the online version of this article at the publisher's web site:
Appendix S1. Detailed materials and methods.
Fig. S1. Representative TEM images of A549 cells cultured at 13% (top panel) and 21% (bottom panel) O_2.
Fig. S2. Figures to illustrate the effect of different culture conditions on ROS generation in A549 cells over 4 h exposure to CuO nanoparticles surface area dose (A to E; 0.0002 to 2 $cm^2 \cdot cm^{-2}$).
Fig. S3. Effect of hydrogen peroxide and diethyl maleate on ROS generation and glutathione depletion respectively.
Table S1. Review of studies comparing the impact of culturing cells under atmospheric and physiological oxygen tensions.
Table S2. Details of the genes selected to examine the hierarchical response of airways cells to oxidative stress, together with previous reports that they are responsive to nanoparticulate challenge.
Table S3. The statistical significance for the change in gene expression between cells cultured under 13% and 21% oxygen following CuO nanoparticle treatment compared against their respective medium controls (no NP treatment).
Table S4. Properties of CuO NP as supplied by manufacturer.
Table S5. Particle size of copper oxide nanoparticles in water or cell culture medium containing no foetal bovine serum (FBS) or at concentrations of 2% v/v (CCM_{FBS2}) over a period of 6 h.